FULL PAPER

Dalton
www.rsc.org/dalton

Computer simulation of nickel in blood-plasma following the *in vitro* investigations of complex formation chemistry with polyamine(amide) ligands

Edmund T. Nomkoko,[a] Graham E. Jackson,*[b] Bandile S. Nakani[a] and Susan A. Bourne[b]

[a] *Department of Chemistry, University of Transkei, Private Bag X1, Unitra, Umtata 5117, South Africa*

[b] *Department of Chemistry, University of Cape Town, Rondebosch 7700, South Africa. E-mail: jackson@science.uct.ac.za; Fax: +27-021-6897499; Tel: +27-021-6502531*

Received 16th April 2004, Accepted 28th April 2004
First published as an Advance Article on the web 18th May 2004

In- and out-of-cell potentiometric techniques have been used to determine the formation constants for nickel(II) with 3,3,9,9-tetramethyl-4,8-diazaundecane-2,10-dione dioxime (L^1), *N*,*N*′-bis(2-hydroxyiminopropionyl)propane-1,3-diamine (L^2) and 1,15-bis(*N*,*N*-dimethyl)-5,11-dioxo-8-(*N*-benzyl)-1,4,8,12,15-pentaazapentadecane (L^3) at 25 °C and an ionic strength of 0.15 mol dm^{-3}. Nickel(II) forms stable complexes with L^1 and L^2 where square-planar $[NiLH_{-1}]$ and $[NiLH_{-2}]$ species predominate under alkaline conditions. The square-planar coordination of nickel by L^1 has been confirmed by a single-crystal X-ray structure, UV/Vis spectrometry and molecular mechanics calculations of the $[NiL^1H_{-1}]$ complex. The introduction of a third amine group into L^3 dramatically decreases the ligand's ability to complex Ni(II). This results from a change in structure of the complex which decreases the ability of the metal ion to promote the dissociation of the amide protons. Using a model of blood plasma, the high binding ability of L^1 towards Ni(II) is calculated to decrease the mobilisation of Cu(II) in plasma by approximately 65%. $[CuL^1H_{-1}]$ is currently under investigation as an anti-inflammatory agent.

Introduction

Nickel has long been recognised as an essential constituent of the catalytic center of four different types of enzymes, namely urease in plants, hydrogenase, CO dehydrogenase and methyl CoM reductase in some strains of bacteria.[1] Contrary to previous assertions that nickel is toxic to higher animals, accumulated evidence suggests that just like copper, nickel is an essential trace element.[1] In fact, nickel has recently been observed to be present as a constituent of a blood serum protein in higher animals such as man and rabbit[1] although no specific role for the metal ion has so far been suggested. Nickel toxicity, therefore, should be linked to the uptake or exposure to high concentrations of the metal ion and hence the alteration of the normal level of nickel in blood. The documented carcinogenic effects of nickel, for example, are believed to arise from absorption or exposure to its dust or its carbonyl complex formed in refinery processes.[1] Recently, nickel has been observed to be capable of activating or inhibiting a number of enzymes, altering membrane properties and influencing oxidation and reduction processes *in vivo*.[1] A typical human diet contains 0.3–0.5 mg of nickel per day with vegetables, oatmeal, dried beans and peas, nuts and chocolate being the main source of this daily intake. There are no reported side effects of this dietary intake but the metal ion's bioavailability depends on its speciation.

We have recently investigated the solution chemistry of Cu^{2+}, Zn^{2+} and Ca^{2+} with 3,3,9,9-tetramethyl-4,8-diazaundecane-2,10-dione dioxime (L^1), *N*,*N*′-bis(2-hydroxyiminopropionyl)propane-1,3-diamine (L^2) and L^3 {1,15-bis(*N*,*N*-dimethyl)-5,11-dioxo-8-(*N*-benzyl)-1,4,8,12,15-pentaazapentadecane} (Fig. 1) for possible use of the resulting copper(II) complexes as anti-inflammatory drugs in the treatment of rheumatoid arthritis.[2–6] Zn^{2+} and Ca^{2+} were included in the study since these metal ions are potential competitors of Cu^{2+} *in vivo*.[7,8] The potentiometric results indicated that copper(II) forms reasonably stable complexes with all three ligands.[2–6] Blood-plasma simulation studies, on the other hand, predicted that only L^1 and L^2 are capable of mobilising copper *in vivo* with little or no interference from Zn^{2+} and Ca^{2+}.[3–6] Biodistribution experiments on mice revealed that indeed the injected radiolabeled ^{64}Cu $[CuL^1H_{-1}]$ and $[CuL^2H_{-1}]$ complexes do not dissociate *in vivo*.[3–6] Although the free nickel(II) ion is present in blood-plasma in negligible concentrations,[7,8] a high dietary intake of nickel could affect the concentration of the administered copper anti-arthritic agents. To this end, formation constants of nickel(II) with all three ligand systems were investigated potentiometrically.

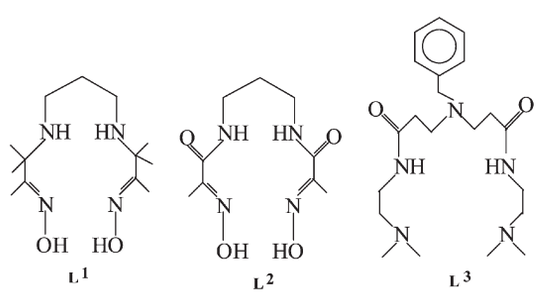

Fig. 1 Structures of studied ligands.

Slow kinetics posed some problems in the determination of the stability constants for Ni(II) with L^1 and L^2. Unlike the copper(II)- and zinc(II)-systems,[2–6] nickel(II) solutions did not reach equilibrium within a reasonable time. This was observed as a drift in potential during the normal titration procedure. The out-of-cell potentiometric technique first explored by Micheloni *et al*.[9] is ideally suited for systems which do not reach equilibrium rapidly. In this paper, we present in- and out-of-cell potentiometric and UV/Vis spectrophotometric studies of the Ni(II)–L^1, –L^2 and –L^3 systems. Blood-plasma simulation studies were performed to assess the ability of the metal to alter the bioavailability of the copper complexes previously investigated. A solid-state investigation and molecular dynamics (MD) simulations of $[NiL^1H_{-1}]^+$ were also carried out in order to ascertain the possible geometries of the nickel(II) species in solution.

Results and discussion

Potentiometry

In an attempt to circumvent the problems of slow kinetics, the Ni(II)–L^1 and –L^2 systems were investigated by an out-of-cell potentiometric technique.[9,10] Only one titration was performed for Ni(II)–L^1 system. The data obtained from this single titration were

DOI: 10.1039/b405756m

Table 1 Formation constants, $\log\beta_{pqr}$, for L^1, L^2 and L^3 with H^+ and Ni(II) studied at 25°C and I = 0.15 mol dm^{-3} (Cl^-).[a,b] σ_{pqr} denotes the standard deviation in $\log\beta_{pqr}$; R_H is the Hamiltonian R-factor and n is the number of titration points. The general formula of a complex is $M_pL_qH_r$

L	Metal	p	q	r	$\log\beta_{pqr}$	σ_{pqr}	n	pH range	R_H
L^1	H^+	0	1	1	8.97	0.002	703	2.2–10.8	0.001
		0	1	2	16.17	0.004			
L^2	H^+	0	1	1	10.408	0.001	975	2.0–11.0	0.004
		0	1	2	20.072	0.001			
L^3	H^+	0	1	1	8.823	0.010	943	2.0–11.0	0.012
		0	1	2	17.254	0.008			
		0	1	3	24.152	0.012			
L^1	Ni(II)[c]	1	1	0	11.530	0.060	60	2.9–10.5	0.008
		1	1	−1	7.621	0.032			
		1	1	−2	−2.201	0.030			
L^2	Ni(II)[c,e]	1	1	1	15.46	0.035	656	2.50–11.0	0.017
		1	1	−1	2.842	0.010			
		1	1	−2	−8.368	0.035			
L^3	Ni(II)[d]	1	1	2	23.280	0.072	465	2.40–10.5	0.065
		1	1	1	16.100	0.103			
		1	1	0	7.570	0.014			
		1	1	−2	−9.640	0.030			

[a] Protonation and [b] complexation titrations involved ligand concentrations of 2.0–8.0 × 10^{-3} mol dm^{-3} and 1.0–6.0 × 10^{-3} mol dm^{-3}, respectively, with metal-to-ligand molar ratios of 1 : 2, 1 : 3, 1 : 4 and 1 : 5. For metal-to-ligand molar ratios of 1 : 1 and 2 : 1 precipitation was observed. Data obtained by [c] out-of-cell and [d] in-cell potentiometric techniques. [e] $\log\beta_{11-1}$ = 1.14 and $\log\beta_{11-2}$ = −7.05 for the Ni–L^2 system have been previously reported.[21]

then combined with potentiometric data initially gathered by a normal automatic titration procedure where the maximum delay time was extended to 60 min between data points.

Complex formation and deprotonation functions

Stability constants obtained by the out-of-cell potentiometric technique are always regarded as estimates because of the uncertainties in the standard electrode potential (E^0) associated with the various solutions. The reliability of the $\log\beta_{pqr}$ values was verified by complex formation ($\bar{Z}_M$) and deprotonation ($\bar{Q}_M$) functions where the former measures the average number of ligands bound per metal ion while the latter indicates the number of protons released due to complexation.[11] Theoretically, the complex formation function is expected to level off at a $\bar{Z}_M$ of 1 for mononuclear ML species formation. Fig. 2 for the Ni(II)–L^2 system shows that $\bar{Z}_M$ levels off at 1.5 because the ML complex is not the predominant species. de Witt *et al.*[12] have recently reported a similar complexation phenomenon. The fanning back of the complex formation function at low pL (−log [L]) values suggests the presence of hydroxo complexes of 11−1 and 11−2 stoichiometry.[13] This fanning back has also been observed with both Cu^{2+} and Zn^{2+}–L^1 and –L^2 systems.[3–6]

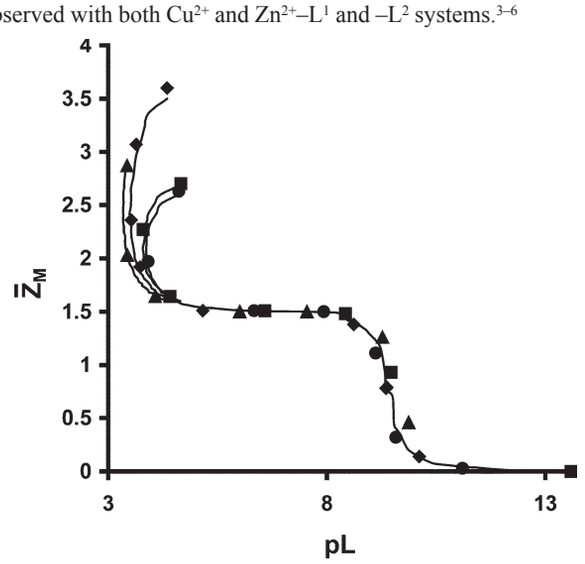

Fig. 2 Experimental and theoretical $\bar{Z}_M$ curves for the Ni(II)–L^2 system; M : L ratios 1 : 2 (■), 1 : 3 (◆), 1 : 4 (▲) and 1 : 5 (●) were used. The theoretical line was calculated using the model given in Table 1.

The $\bar{Q}$ function given in Fig. 3 for the Ni(II)–L^2 system increases from 0 at pH 5 to a maximum value of 3 at pH 7.0. Since in this pH range the ligand is diprotonated (see $\bar{n}$ curve), loss of three protons results in the formation of the 11−1 species. Above pH 7.5 the $\bar{Q}$ function runs parallel to the $\bar{n}$ curve indicating that no protons are gained or lost due to complexation. Above pH 10, the two curves diverge again indicating the further loss of a proton to form the 11−2 species. This complexation pattern is reflected in the speciation plot (Fig. 4) constructed using the constants evaluated below. We have observed a similar complexation pattern for Ni(II) with L^1. Despite the known limitations associated with slow kinetics as observed for the Ni(II)–L^1/L^2 systems, Figs. 2 and 3 show excellent agreement between the experimental and calculated functions for varying M : L ratios. This agreement lends confidence to the model obtained in the data analysis.

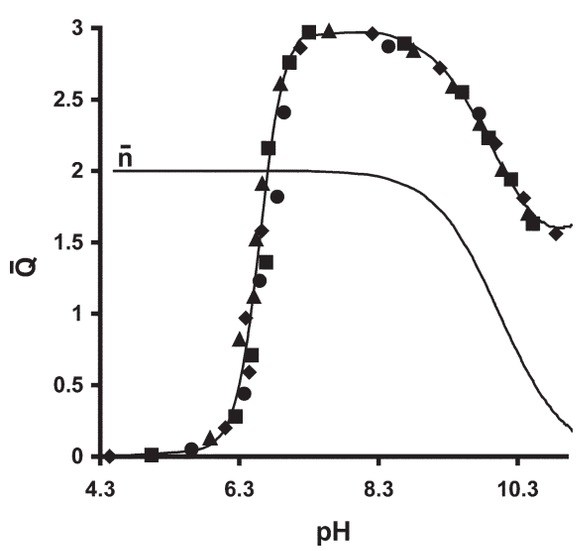

Fig. 3 Experimental and theoretical $\bar{Q}$ and $\bar{n}$ curves for the Ni(II)–L^2 system; M : L ratios 1 : 2 (■), 1 : 3 (◆), 1 : 4 (▲) and 1 : 5 (●) were used. The theoretical line was calculated using the model given in Table 1.

Formation constants

Data analysis using the ESTA suite of computer programs[11,14,15] yielded the $\log\beta_{pqr}$ values given in Table 1. The ligand L^2 coordinates strongly to Ni(II) as indicated by $\log\beta_{111}$ = 15.460, $\log\beta_{11-1}$ =

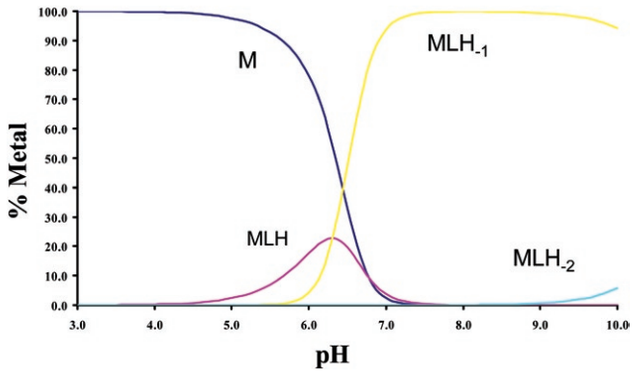

Fig. 4 Speciation diagram for the Ni(II)–L^2 system; $[Ni]_{total} = 0.00333$; $[L^2]_{total} = 0.01$ mol dm^{-3}.

2.842 and $\log\beta_{11-2} = -8.368$ for 111, 11−1 and 11−2 species, respectively. Stability constant values for these systems are not unreasonable, as nickel(II) always forms relatively stable complexes with ligands that bind strongly to copper(II) and zinc(II). In fact, higher stability constants for nickel(II)–L^1 and –L^2 complexes compared to the corresponding zinc(II) species,[3–6] result from the additional ligand field stabilisation due to formation of spin-paired square-planar complexes containing four strong Ni(II)–N σ bonds. In solution, it is postulated that two water molecules remain coordinated axially to copper(II) and zinc(II), while nickel(II) sheds all six water molecules on coordination to L^1 and L^2 in the $[NiLH_{-1}]$ and $[NiLH_{-2}]$ complexes. In addition to these hydroxo complexes, the double positively charged $[NiL^1]$ species is believed to be square-planar. Hence, $\log\beta_{pqr}$ values in these Ni(II)–L complexes include the ligand-field effects of square-planar, MN_4, coordination. For the $[NiLH_{-1}]$ complexes, an additional stabilisation would be expected to be achieved by formation of a short intramolecular hydrogen-bond between the two terminal oxime oxygen atoms, which is typical of bis(oximato) complexes.[16] Here, the coordination is described as pseudo-macrocyclic.[2–6]

Unlike the copper and the zinc systems where the formation of the neutral $[ML^1H_{-2}]$ complex species is associated with the loss of the proton from a water molecule, with nickel, the short intramolecular hydrogen-bond observed in the pseudo-macrocyclic $[ML^1H_{-1}]$ species is believed to break releasing a proton into the solution. The first and second calculated nickel(II) promoted deprotonation of the dione dioxime groups (pK_{M-NOH}) in the L^1 system are 3.92 and 9.47 in moving from $[NiL]$ to $[NiL^1H_{-2}]$ *via* $[NiL^1H_{-1}]$, respectively. These pK_{M-NOH} values indicate that the proton(s) are indeed lost from the terminal oxime groups rather than from axially bound water molecules. In fact, the loss of these protons is easier by approximately 8.3 and 2.8 log units compared to the free ligand ($pK_a \approx 12.3$)[17] indicating the involvement of the metal ion in this process.

The Ni(II)–L^2 complexation begins with the formation of the $[NiL^2H]$ complex where the ligand is believed to be coordinated to the metal ion through one amide nitrogen and one oxime oxygen atoms. In this protonated $[NiL^2H]$ species, the other four nickel(II) binding sites are presumed to be occupied by water molecules. The simultaneous loss of two protons (one from the second amide group and the other from one of the oxime moieties) from the $[NiL^2H]$ complex results in the formation of the square-planar $[NiL^2H_{-1}]$ species where all four nitrogen donor atoms of the ligands are coordinated to the metal ion. Above pH 8.5, the hydrogen bond in $[NiL^2H_{-1}]$ is believed to break releasing the proton into solution. This leads to the $[NiL^2H_{-2}]$ complex. The metal promoted simultaneous deprotonation of the amide and oxime groups ($pK_{M-CONH-NOH}$) is given by the difference between $\log\beta_{111}$ and $\log\beta_{11-1}$, which for L^2, is 12.62. The pK_{M-CONH} and pK_{M-NOH} values of 5.164 and 7.454 can be assigned to the metal ion-assisted deprotonation of the amide and oxime groups, respectively. We have previously[6] reported a pK_{M-CONH} value of 4.17 for copper(II) with L^2. The pK_{M-CONH} value of 5.16 for the nickel(II) system is in the range expected for deprotonation of the amide moiety.[18,19] The loss of a proton from an oxime group coordinated to a met al ion ($pK_{M-NOH} = 7.454$) is 2.5–3.0 log units easier than the deprotonation of an oxime group of the free ligand ($pK_{a1} = 9.664$) or the hydrolysis constant of a coordinated water molecule[20] whose $\log\beta_{10-1} = -10.20$. A square-planar geometry of the ligand could be further stabilised by hydrogen bonding between the two oxime groups to form a pseudo-macrocyle. The second oxime proton is postulated to be lost during formation of $[NiL^2H_{-2}]$ ($pK_{M-NOH} = 11.21$). The loss of the second proton from the complex is approximately one log unit more difficult that the loss of a proton from the free ligand ($pK_{a2} = 10.408$). This supports the idea that the proton is hydrogen bonded in the complex.

Duda *et al.*[21] never observed the presence of the protonated $[NiL^2H]$ species. In addition, the presently evaluated formation constants for $[NiL^2H_{-1}]$ and $[NiL^2H_{-2}]$ are two log units higher than those reported by these researchers.[21] This large difference cannot be accounted for by the small difference in background electrolyte used in the two studies (0.10 mol dm^{-3} KCl was used by Duda *et al.*[21]). Furthermore, these authors reported that equilibrium is reached instantaneously. This is in sharp contrast to the slow kinetics observed in the present investigations, where long delays were required between titration points in order to allow the system to come to equilibrium.

In contrast to the Ni(II)–L^1/L^2 systems mentioned above, the metal ion appears to coordinate only weakly to L^3. In fact, the $\bar{Z}_M$ and $\bar{Q}$ values remain close to 0.0 throughout the pH and ligand concentration range investigated. One of the reasons for this weak binding is related to the difficulty associated with the deprotonation of the amide nitrogens. The speciation plots indicate that the protonated 112 ($\log\beta_{112} = 23.28$) and 111 ($\log\beta_{111} = 16.10$) species dominate in the pH range 2.5–8.3. The metal assisted deprotonation of either a coordinated water molecule or an amide nitrogen occurs above pH 7.0 leading to the formation of the 110 species with $\log\beta_{110} = 7.57$. The 110 species can also be formed by the coordination of the three tertiary amines. The calculated $pK_{ML-OH} = 8.53$ is close to the second protonation constant of the free ligand ($pK_{a2} = 8.43$) and 1.5 log units lower than the hydrolysis constant of the metal ion ($pK_{M-OH} = 10.20$).[20] This indicates that the proton is more likely to have been released from the amide group. The deprotonation of the amide moiety of the ligand by Cu^{2+} has been observed to be 2 log units easier[3] than the hydrolysis of a coordinated water molecule.[20] Another noticeable feature about the complexation behaviour of this system is the absence of the 11−1 complex. Instead, above pH 8.5 the 11−2 complex with $\log\beta_{11-2} = -9.64$ predominates. This can be explained in terms of the pH delayed coordination of either the second amide nitrogen or both amide groups if the terminal nitrogens are coordinated in the 110 species. If the latter assumption is true, this behaviour is reminiscent of complexation chemistry of some linear tetraamines[18] and most macrocyclic dioxo tetraamine ligands[19] where the 11−1 species is normally present as a minor species. If the neutral $[NiL^3H_{-2}]$ is formed by deprotonation of the amide groups, it is believed to be further stabilised by the coordination of the fifth terminal nitrogen in an axial position. However, this increased stability is offset by the formation of contiguous six-membered chelate rings. The possibility of formation of a mixture of the above proposed $[NiL^3H_{-2}]$ complexes in solution cannot be ruled out. It should be mentioned that the pH range investigated was limited to <9.0 because precipitation of the neutral $[NiL^3H_{-2}]$ species occurred above this pH value.

Amendola *et al.*[22] have recently designed and studied the solution chemistry of a two compartmental ligand capable of binding Ni(II) in a pH dependent manner. In weakly acidic or basic conditions, the metal ion resides in a compartment containing two quinoline nitrogens and two amino nitrogen donor atoms. Above pH 8.0, Ni(II) translocates into the compartment containing amide and amino groups. The development of these ditopic ligands is important in keeping the metal ion in solution until a high pH is reached for the metal ion facilitated ionisation of the amide groups to occur. These observations support the solution behaviour observed for Ni(II) with L^3.

The degree of metal–ligand complexation, as judged by stability constants, is a complex phenomenon governed by many factors. These include amongst others the nature and the spatial arrange-

ment of donor atoms comprising the ligand, its denticity,[23] the extent of its preorganisation,[24,25] the nature of the rings formed due to complexation and the metal ion concerned. Subtle changes in the ligand backbone such as the incorporation of pendant arms, can have an influence on the coordination behaviour of the ligand towards a particular metal ion.[21] Two factors of importance in most ligand systems, which are not always evident in aqueous complex formation are: (i) the role of steric hindrance to complexation[26,27] and (ii) the degree of pre-organisation of the ligand to enhance complexation.[24,25] Steric hindrance results in a lowering of the complex stability and in highly unfavourable instances results in the total exclusion of the metal ion by such a ligand.

It has been observed that a preorganised ligand such as cyclam (1,4,8,11-tetraazacyclotetradecane) requires minimum structural changes to become coordinated to a metal centre.[25] Steric hindrance and the degree of pre-organisation present in the ligand system may contribute significantly to the thermodynamics and kinetics of metal–ligand complexation. In fact, Hancock *et al*.[26] noted that cyclam, in complexation with Ni(II), forms rapidly a *trans*-I (*RSRS*) conformer which is then slowly converted to the stable *trans*-III (*RSSR*) conformer after deprotonation at a nitrogen. For both TMC (1,4,8,11-tetramethyl-1,4,8,11-tetraazacyclotetradecane)[10] and TPTA {1,4,8,11-tetrakis(diphenylphosphinomethyl)-1,4,8,11-tetraazacyclotetradecane},[28] Ni(II) assumes a square-pyramidal geometry corresponding to the *trans*-I (*RSRS*) conformer. However, this *trans*-I (*RSRS*) conformer does not undergo an inversion at a nitrogen to form the *trans*-III (*RSSR*) conformer that is observed with cyclam because of the absence of hydrogens on the nitrogen donor atoms.

Hay and Norman[29] predicted that complex formation in both copper– and nickel–TMC systems occurs in a two-step process: (i) the initial rapid reaction between $[M^{2+}]$ and [L] which is first order in both components giving rise to the unstable intermediate $[ML]^{2+}_{int}$ and (ii) the subsequent much slower step which is independent of both $[M^{2+}]$ and [L] but first order with respect to $[ML]^{2+}_{int}$ and first order overall. In acetonitrile,[29] N-methylation and C-methylation of cyclam affects the rate of the initial second-order reaction only to a small extent, whereas in coordinating solvents[30] such as *N*,*N*-dimethylformamide (DMF) and dimethyl sulfoxide (DMSO), the reaction of Ni(II) with TMC is much slower than it is with cyclam. The nature of the intermediate $[ML]^{2+}_{int}$, has not been studied in detail, consequently the mechanism of the slow step is still not fully understood.

Roper and Elias[31] through kinetic studies on these reactions, have postulated that the intermediate is in a *trans*-II (*RSRR*) configuration of form $[Ni(TMC)(S_2)]^{2+}$ where S is the solvent molecule. In this intermediate, two solvent molecules are still coordinated axially to the metal ion. The *trans*-II (*RSRR*) $[Ni(TMC)(S_2)]^{2+}$ complex, through nitrogen inversion, is ultimately converted to the stable *trans*-I (*RSRS*) species. This step is rate limiting. The Ni(II)–N bond inversion is believed to be accompanied by a loss of a solvent molecule. The absorption spectrum of this intermediate species indicates planar N_4 coordination and is very close to the geometries of the final products in the *trans*-I (*RSRS*) configured $[ML]^{2+}$ species. It has been observed that intermediate formation with copper(II) and its subsequent rearrangement is ten times faster than nickel(II).[31] It is believed that in the course of the rather fast process of intermediate formation there is not enough time for the ligand to accommodate the metal ion in the thermodynamically most stable state.[9,31]

L^1 and L^2 share similar characteristics with TMC and TPTA in that the methyl groups in position 3 and/or 9 should create similar steric effects to those of N-methylated analogues. In light of the introductory remarks and the foregoing discussion, it is proposed that the slow kinetics of nickel(II) with L^1 observed in this study is a consequence of both steric hindrance to complexation and the conformational changes demanded by the metal ion. In addition to low levels of pre-organisation, for L^2 the slow kinetics is further enhanced by the difficulty associated with the deprotonation of the amide groups. It is, therefore, the presence of the metal ion, which reorganizes the ligands to adopt conformations that will promote complexation. These abilities are properties of a particular metal ion and will differ from one metal to another as observed in previous investigations with copper[3–6] and in this study with nickel and in kinetic experiments with both metal ions.[31] For L^3, it has been difficult to measure with great accuracy the degree of metal–ligand binding because of the difficulty with which nickel(II) deprotonates the amide nitrogens.

Blood-plasma simulation studies

Thermodynamic data, in the form of formation constants, have been used in computer models to predict the effect of a particular component on a large number of interrelated systems. One such model is the ECCLES blood-plasma model which contains approximately 40 ligands and ten metal ions making up roughly 5000 complexes.[7,8] The reliability of any output from any model depends on the input data. This is the reason why the meticulous investigation of formation constants is needed. The effect of Ni(II) on the ability of the ligands to mobilise copper(II) *in vivo* was investigated by incorporating the relevant constants into the model and calculating blood-plasma mobilising indices (pmi's). The pmi of a particular metal ion is defined as the ratio of the total concentration of low molecular mass (lmm) metal species in the presence and the absence of a ligand. Fig. 5 shows the results of such a calculation. Note the absence of any significant mobilisation of Ni(II) by L^2 and L^3. This is expected because the Ni(II) formation constants with these ligands are 8–9 log units lower than those of Cu^{2+}. L^1 causes significant mobilisation of Ni(II), increasing its low molar mass fraction 10-fold at a concentration of 10^{-4} mol dm^{-3}.

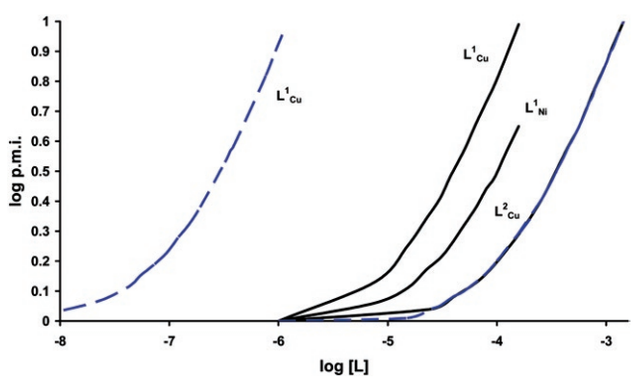

Fig. 5 Cu^{2+} and Ni(II) pmi's plotted as a function of the ligand concentration. The solid lines are calculated in the presence of 1.8×10^{-14} M Ni(II) while the dashed lines are calculated in the absence of any Ni(II).

In the absence of Ni(II), at μmol concentrations, L^1 is calculated to increase the lmm concentration of Cu(II) in blood plasma 10-fold. However, in the presence of 10^{-14} M Ni(II), a concentration of 10^{-4} mol dm^{-3} of L^1 is needed to achieve the same increase in lmm Cu(II). This decrease in mobilisation is due to the competition between Cu(II) and Ni(II) for the added L^1. For comparison, the results for L^2 are given in Fig. 5. Here, no significant Ni(II) complexation occurs and so the Cu(II) pmi curves in the presence and absence of Ni(II) are superimposable.

UV/Vis spectroscopy

Because of the slow kinetics of the nickel(II)–L^1/L^2 systems, solutions of differing hydrogen ion concentrations were equilibrated for a maximum of three weeks before measurements were taken. As an indicator that the systems had reached equilibrium, UV/Vis spectrophotometric measurements revealed the absence of bands associated with hydrated Ni(II). Above pH 3.5, both the Ni(II)–L^1 and –L^2 systems exhibit a single absorption band centred at about 426.5 and 377 nm, respectively. To gain more insight into the coordination geometries of the nickel(II)–L^1 and –L^2 complexes, spectral deconvolution was performed using a local BASIC program to solve the expanded Beer–Lambert relationship. In this way, spectra of the individual species present in solution could

Table 2 The UV/Vis spectra data for Ni(II)–L^1 and –L^2 complexes determined at room temperature using water as a solvent[a]

Complex	λ_{max}/nm	ε/mol^{-1} dm^3 cm^{-1}
[NiL^1]	426.5	45
[NiL^1H_{-1}]	426.5	80
[NiL^1H_{-2}]	426.5	103
[NiL^2H][b,c]	—	—
[NiL^2H_{-1}][b]	475	170
[NiL^2H_{-2}][b]	455	380

[a]The reported bands are the d–d transitions and [b]an LMCT band at 377 nm with ε of approximately 2000 mol^{-1} dm^3 cm^{-1} is observed for all Ni–L^2 complexes and is assigned to the N^- (deprotonated amide nitrogen) $\rightarrow {}^1A_{2g}$ transition. [c]The three bands normally expected for Ni(II) in an octahedral environment are obscured by this LMCT band.

be obtained. The analysis is based on the equilibrium constants measured in this study and since each wavelength is treated independently, the fact that smooth curves are obtained for the spectra of the individual species and the fact that the experimental spectrum of $[Ni(H_2O)]^{2+}$ is faithfully reproduced, lends confidence to the potentiometric results.[2] Table 2 gives a summary of λ_{max} and the associated molar extinction coefficients. The [NiL^1], [NiL^1H_{-1}] and [NiL^1H_{-2}] complexes exhibit a single band centred at about 426.5 nm (23850 cm^{-1}) with molar extinction coefficients of 45, 80 and 103 mol^{-1} dm^3 cm^{-1}, respectively. Vassian and Murmann[32] reported a λ_{max} of 423 nm for the [NiL^1H_{-1}]ClO_4 complex (ε = 130 mol^{-1} dm^3 cm^{-1}) which is in good agreement with the absorption maximum and molar absorptivity obtained in this study for the same species. Two weak broad bands at 475 nm (ε = 170 mol^{-1} dm^3 cm^{-1}) and 455 nm (ε = 380 mol^{-1} dm^3 cm^{-1}) are seen for the hydroxo [NiL^2H_{-1}] and [NiL^2H_{-2}] complexes, respectively, as a shoulder on a prominent ligand to metal charge transfer (LMCT) transition. The d–d transitions fall in the predicted 420–480 nm wavelength region with molar absorptivities of 120–500 mol^{-1} dm^3 cm^{-1} expected for square-planar complexes.[33,34] The single absorption band for these complexes constitutes the ${}^1A_{2g} \leftarrow {}^1A_{1g}$ and ${}^1B_{1g} \leftarrow {}^1A_{1g}$ transitions typical of square-planar Ni(II) species.[33] As expected, the protonated 111 ([NiL^2H]) complex, which is postulated to be octahedral, does not exhibit a band in the afore-mentioned wavelength range predicted for square-planar Ni(II) complexes.

The prominent band centred at 377 nm for the Ni(II)–L^2 system is an LMCT transition originating either from the carbonyl oxygen, deprotonated amide nitrogen or the oxime nitrogen to the vacant ${}^1A_{2g}$ orbital of the metal ion. The molar extinction coefficient of this band for the 111, 11−1 and 11−2 species is in the range of 1785.7–2500 mol^{-1} dm^3 cm^{-1} in support of its charge transfer (CT) character. Duda *et al.*[21] have also observed CT transitions at 301 (sh), 369 and 399 (sh) nm for the [NiL^2H_{-1}] and [NiL^2H_{-2}] complexes where the former and the latter bands are seen as shoulders. Unfortunately, no account of the origin of these CT transitions was given by these authors. Bojczuk *et al.*[35] have proposed three O^-, N^- and $NH_2 \rightarrow Cu^{2+}$ charge-transfer transitions which lie at 385, 327 and 277 nm, respectively. The intra-ligand $\pi \rightarrow \pi^*$ transition, on the other hand, occurs around 250 nm.[21] Such a CT transition has not been observed in the Ni(II)–L^1 system which contains both the coordinated amino and deprotonated oxime groups. This suggests that this band is neither due to $O^- \rightarrow Ni$(II) nor $NH_2 \rightarrow Ni$(II) electronic transition. Ni(II) has been found to be capable of deprotonating the amide groups of L^2 which are absent in L^1. We believe that this LMCT band is due to an electron transition from the deprotonated amide nitrogen (N^-) to the vacant ${}^1A_{2g}$ orbital of the metal ion. This (N^-)$\rightarrow$Ni(II) transition assignment is further justified by the recognition that the ligand is postulated to be coordinated to the metal ion by a deprotonated amide nitrogen and oxime oxygen in the [NiL^2H] complex where the same CT band has been observed.

There is no evidence of further absorption above 500 nm in both the Ni–L^1 and –L^2 systems, which is typical of square-planar nickel(II) complexes.[33] The ligands form 5,6,5 (110 and 11−2 species) and 5,6,5,6 (11−1 complex) membered chelate rings (Fig. 6) around the small, diamagnetic Ni(II) ion. Electronic spectra of Cu^{2+}complexes of 3,3,8,8-tetramethyl-4,7-diazadecane-2,9-dione dioxime (EnAO)[2] and 4,4,9,9-tetramethyl-5,8-diazadodecane-2,11-dione dioxime (H_2tmdddo)[17] indicate that dissociation of an oxime proton causes an increase in the donor strength of the oxime nitrogen atom. There is no red shift in the d–d transition upon formation of [NiL^1H_{-2}] from [NiL^1H_{-1}]. Furthermore, no blue shift has been observed in λ_{max} on moving from [NiL^1] to the pseudo-macrocyclic [NiL^1H_{-1}] complex. This suggests that, in these complexes the stabilisation of the square-planar geometry is determined mostly by the presence of three fused chelate rings. In contrast, the formation of the [NiL^2H_{-2}] from [NiL^2H_{-1}] species is associated with a 20 nm decrease in λ_{max}. This behaviour can be viewed as originating from the stronger electron donating power of two deprotonated oxime groups. The hydrogen bond is believed to play a less significant role in these nickel(II) species compared with copper(II)–oxime ligand complexes.[2,17] In fact, the NH–$CH(CH_3)_2CH(CH_3)$N–OH fragment in L^1 and NH–COCHN–OH moiety in L^2 can be viewed as electron sinks for metal ions such as Ni(II), which are capable of deprotonating the oxime and/or amide groups.

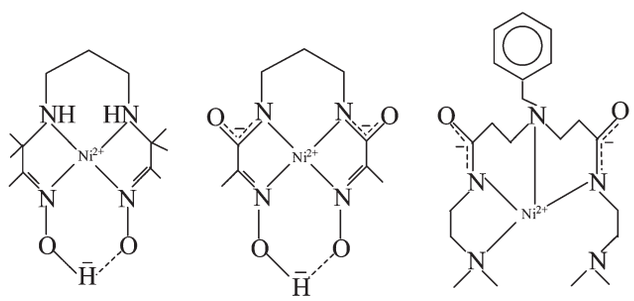

Fig. 6 Proposed structures of the [$NiL^{1/2}H_{-1}$] and [NiL^3H_{-2}] species in solution. For simplicity, the axial H_2O ligands are omitted in the [NiL^3H_{-2}] representation.

In contrast to the above observations, nickel does not seem to deprotonate the amide nitrogens of L^3. In fact, the hydrated Ni(II) and the protonated 112, 111, 110 complexes predominate in the whole acidic to neutral pH region before the onset of precipitation. It seems the above-mentioned potentiometrically detectable species are too weak to absorb appreciably in the 340–800 nm wavelength range. As a result, no information could be obtained from the absorption spectra of these complexes. Moreover, Ni(II) does not seem to form the positively charged 11−1 species with L^3, which has been detected in the corresponding Cu^{2+} system.[3] If it were to form in solution, the mono-positively charged [NiL^3H_{-1}]$^+$ complex would be expected to absorb appreciably in the wavelength range studied.

Solid state studies

UV/Vis spectrophotometry predicted the geometries of the studied Ni(II)–L^1/L^2 systems fairly accurately. However, the proposed structures given in Fig. 6 do not give any information about the lowest possible energy conformations. Furthermore, the orientation of the alkyl substituents relative to the molecular plane defined by the ligand's donor atoms is unknown. In order to assess fully the coordination nature of L^1, L^2 and L^3 towards the metal ion, attempts were made to isolate crystals of the [$NiLH_{-1}$] species. However, these investigations were unsuccessful and only the [NiL^1H_{-1}]$^+$ species was isolated. This cationic species (Fig. 7) crystallised as a perchlorate salt with a molecular formula $C_{13}H_{27}ClN_4NiO_6$.

A search of the Cambridge Structural Database[36] revealed 10 crystal structures involving L^1. Of these, one is of the ligand alone (CSD refcode CEYSOO) while only one involves square-planar coordination to a metal ion. This (CSD refcode APBXNI) is the chloride hydrate of [NiL^1H_{-1}]$^+$ which was reported by Hussain and Schlemper.[37] The molecular structure of the cation is identical in both APBXNI and [NiL^1H_{-1}]ClO_4: the aza (N5 and N9) and oxime (N2 and N12) nitrogen donor atoms are involved in an equatorial

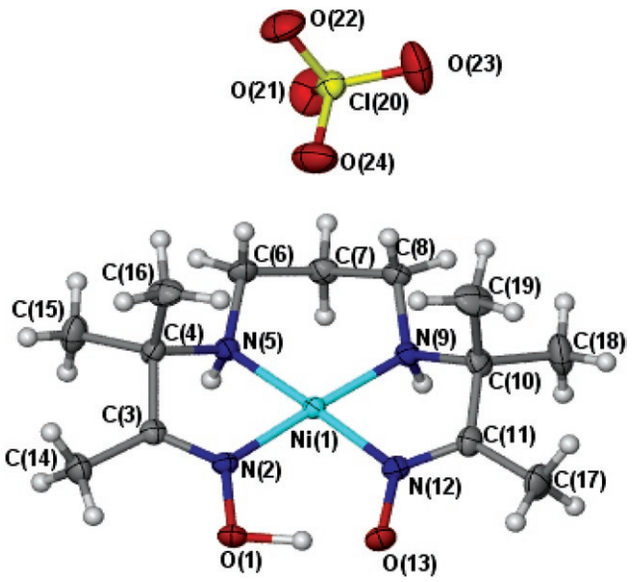

Fig. 7 ORTEP representation of the crystal structure of cationic $[NiL^1H_{-1}]^+$ species and the perchlorate (ClO_4^-) anion showing 50% probability ellipsoids and the atom labelling scheme. Hydrogen atoms are represented as open circles.

coordination to the metal ion with Ni–N_{ox} bond lengths of 1.872(1) and 1.873(2) Å (*cf.* 1.877 and 1.875 Å in APBXNI) and Ni–N_{aza} bond lengths of 1.924(1) and 1.933(1) Å (*cf.* 1.917 and 1.934 Å in APBXNI). In both structures, the Ni lies in a plane with all four nitrogen atoms (rms deviations <0.01 Å) but the six-membered ring formed by Ni1–N5–C6–C7–C8–N9 is in the half-chair conformation with Ni, N5 and N9 in a plane and C7 out of the plane by 0.35 and 0.39 Å for APBXNI and $[NiL^1H_{-1}]ClO_4$, respectively.

As may be expected, the conformation of the ligand alters on complexation; the most notable change being the torsion angle about the backbone N–C–C–N which twists from 125.2° in CEYSOO to 26.0 and −20.9° in APBXNI and 25.2 and −22.2° in $[NiL^1H_{-1}]ClO_4$. Both these studies give credibility to the square-planar geometry inferred in this study from UV/Vis data. The influence of the counter anion is most clearly seen in the crystal packing of the two structures. APBXNI is characterised by cations offset from one another and related by a two-fold screw axis running along (100). In this direction, the layers of cations are separated from one another by a layer of chloride ions and water molecules. An extensive network of hydrogen bonds connects the cations, anions and water molecules (Fig. 8 and Table 3). In contrast, incorporation of the perchlorate ion allows the cations to approach one another more directly and the packing is characterised by hydrogen bonded cation dimers in layers with intercalated perchlorate ions (Fig. 9 and Table 3). In this case, the cations are related by two-fold rotation axes.

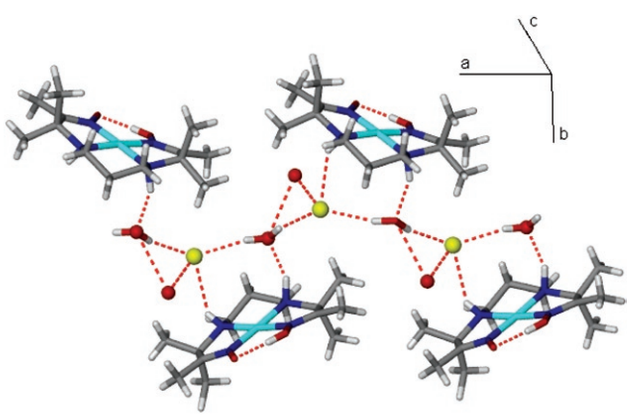

Fig. 8 Packing diagram of APBXNI showing hydrogen bonding connecting offset layers of cations.

As expected, the methyl groups at C-4 and C-10 are staggered due to electrostatic repulsion of the hydrogens. Duda *et al.*[21] recently reported a crystal structure of $Ni(H_2O)_6[NiL^2H_{-1}]_2$, whose Ni–N bond lengths vary between 1.96 and 1.97 Å. In fact, in this $[NiL^2H_{-1}]_2^{2-}$ crystal system, the Ni–N_{am} and Ni–N_{ox} bond lengths are equal to within 0.005 Å. This is an indication of an equal electron donating ability of these nitrogen donor atoms towards the metal ion. Of particular interest is the observation that the Ni–N_{aza} and Ni–N_{ox} bond distances of the $[NiL^1H_{-1}]^+$ crystal system are approximately 0.7 and 0.1 Å, respectively, longer than the corresponding bonds in $[NiL^2H_{-1}]^+$.[21] The shorter Ni–N bonds in L^2 species compared to Ni–L^1 complexes further indicate the high basicity of these nitrogens, hence the observed λ_{max} in the 420–480 nm range observed for square-planar $[NiL^2H_{-1}]$ and $[NiL^2H_{-2}]$.

Table 3 Hydrogen bonding interactions (D = donor, A = acceptor)

D–H···A	D–H	H···A	D···A	D–H···A
APBXNI				
N(1)–H(1)···Cl(1)	0.779	2.662	3.288	139
N(4)–H(2)···O(3)	1.020	1.927	2.888	156
O(1)–H(26)···O(2)	0.857	1.695	2.423	141
O(3)–H(27)···Cl(1)	0.935	2.351	3.225	156
O(3)–H(28)···Cl(1)[a]	0.926	2.362	3.253	161
$[NiL^1H_{-1}]ClO_4$				
N(5)–H(5)···O(13)[b]	0.930	2.155	3.035	157
N(9)–H(9)···O(22)[c]	0.930	2.588	3.332	137
N(9)–H(9)···O(1)[b]	0.930	2.321	3.054	135
O(1)–H(1)···O(13)	1.14	1.30	2.414	171

[a] *via* −1/2 + *x*,1/2 − *y*, −*z*. [b] *via* −*x*, 1 − *y*, 1 − *z*. [c] *via* −*x*, *y* − 1/2, 1/2 − *z*.

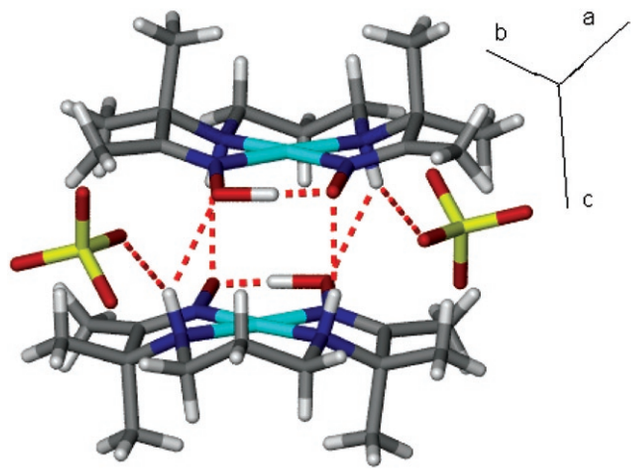

Fig. 9 Crystal packing of $[NiL^1H_{-1}]ClO_4$.

MM calculations and MD simulations of the $[NiL^1H_{-1}]^+$ system

In the absence of suitable crystals for X-ray structure analysis, MM calculations and MD simulations may give some insight about the coordination behaviour of a particular ligand's donor atoms towards a given metal ion. In these calculations care was taken of the preferred coordination geometry of the metal ion. The structure of the $[NiL^1H_{-1}]^+$ species was built and its potential energy minimised using the ESFF forcefield.[37] Molecular dynamics (MD) simulations of this species were run for 5 ps in order to assess the relative orientation of the methyl groups in the energy minimised complex.

Fig. 10(a) and (b) show the crystal structure of $[NiL^1H_{-1}]^+$ superimposed onto the computed structure. As seen from the figure, there is a very good agreement between the experimentally determined structure and the simulated species which is also manifested in bond lengths and angles. One noticeable difference between the two lies with the relative orientation of the propylene bridge separating the aza nitrogens. In the crystal structure this bridge is projecting away form the molecular plane defined by the metal ion and the nitrogen donor atoms of the ligand. The simulated structure, in contrast, has the propylene bridge in the same plane as the metal ion and the coordinated donor atoms. Although there is good agreement in the

$Ni–N_{ox}$ distances between the two species, the $Ni–N_{aza}$ bond lengths (1.97 ± 0.01 Å) in the simulated species are 0.03–0.04 Å longer than those reported in the crystal structure above. This difference is within experimental error. We have recently observed that the in-plane projection of the propylene bridge causes the elongation of the $Zn–N_{aza}$ bonds without affecting the $Zn–N_{ox}$ bond lengths.[5] These studies indicated very little conformational differences between the observed crystal and energy minimised simulated structures. This is an important result in the development of force-fields for modelling of transition metal complexes.

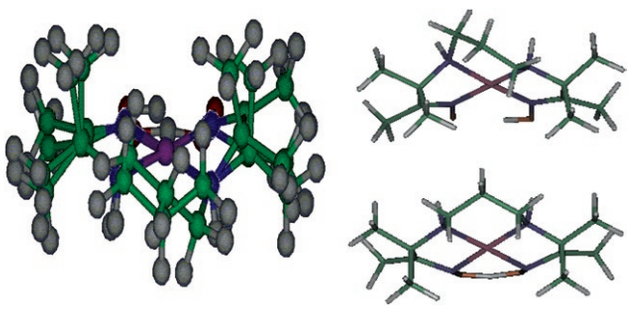

Fig. 10 Superimposed crystal (top) and simulated species (bottom) of $[NiL^1H_{-1}]^+$ in (a) ball and stick model and (b) stick representation (atoms at the crossing points), Color code: Ni(II) – pink, nitrogen – blue, oxygen – red, carbon – green and hydrogen – gray).

Conclusion

The equilibrium constants for nickel(II) with L^1, L^2 and L^3 were investigated using in and out-of-cell potentiometric techniques. Complex formation and deprotonation functions were used as criteria in model selection. Nickel(II) forms stable complexes with L^1 and L^2 where the square-planar pseudo-macrocyclic 11−1 species predominate in neutral conditions. A square-planar arrangement of the ligands' donor atoms around the metal ion has been suggested on the basis of UV/Vis spectrophotometric measurements. This preferred geometry has been confirmed by a single-crystal X-ray structure, MM calculations and MD simulations of the $[NiL^1H_{-1}]$ complex. The slow kinetics which posed problems in the accurate determination of the formation constants by the normal titration procedure can be rationalised in terms of the low levels of pre-organisation exhibited by these ligand systems. For L^1 and L^2, other contributing factors to the slow kinetics may be steric hindrance to complexation by the presence of the methyl groups and the difficulty associated with the deprotonation of the amide moiety. The latter point may also account for the low coordinating ability of L^3 towards the metal ion. A high concentration of the nickel ion in plasma as a result of the intake of foodstuffs rich Ni(II) is predicted to cause more than 60% dissociation of the $[CuL^1H_{-1}]^+$ species, currently under investigation as a promising anti-inflammatory agent for rheumatoid arthritic patients.

Experimental

Potentiometry

The syntheses of the ligands L^1, L^2 and L^3 have been described previously.[2–6] They were characterised spectroscopically and by elemental analysis. The purity of the ligands was checked by potentiometry and found to be greater than 95%. All other reagents were commercially available and of analytical grade and standardized[39] where necessary. All solutions were prepared in glass-distilled, deionised water which had been boiled to remove dissolved CO_2. The carbonate content of the sodium hydroxide titrant solution, in particular, was checked using the Gran method,[40,41] otherwise it was used within a short period of time after preparation and was discarded whenever there were signs of carbonate contamination. An ionic strength of 0.15 mol dm^{-3} Cl^- (Na^+) was maintained throughout the titrations.[2–6] The titration procedure has been described before[5] and the electrode system was calibrated for $[H^+]$ *in situ*. The potentiometric titration data were analysed using the ESTA suite of computer programs.[11,14,15]

It has been indicated earlier that slow kinetics posed some problems in the determination of the stability constants of the nickel(II)–L^1/L^2 systems. The slow kinetics manifested themselves as a potential drift in the pH range 3.0–7.0, and hence an out-of-cell potentiometric technique[9,10] was used to circumvent this problem. Standard solutions containing 0.002 mol dm^{-3} L^1/L^2 and 0.001 mol dm^{-3} Ni(II) were prepared at an ionic strength of 0.15 mol dm^{-3} (Cl^-). 4 cm^3 aliquots of these standard solutions were pipetted into eleven vials. To each vial the following volumes of 0.1 mol dm^{-3} NaOH were added (0.0, 0.05, 0.10,..., 0.40, 0.45 and 0.5 cm^3). These vials were equilibrated at 25.0 ± 0.1°C for about three weeks. After three weeks, the final pH values were then recorded and compared with the values obtained during the course of equilibration. The fact that there were minimal changes in the readings after three weeks compared to those of two weeks of equilibration was considered to be an indication that the system had reached equilibrium. The pH measurements were converted to emf values (mV) and the stability constants evaluated using ESTA.[11,14,15] The Ni(II) and Cu(II) pmi's on inclusion of the formation constants and with the use of the database of May *et al*.[7] were efficiently and conveniently interrogated by the ECCLES program[8] on a PC.

UV/Vis spectroscopy

The pH values and UV visible electronic spectra of the solutions which were equilibrated over three weeks, at 25.0 ± 0.1°C, containing a ratio of Ni(II) : L^1/L^2 = 1 : 3, were recorded. Spectrophotometric measurements were taken at 10 nm intervals in the wavelength range 340–800 nm using the Philips PU 8620 UV/VIS/NIR spectrophotometer, Unicam SP 1700 ultraviolet spectrophotometer (with slit and band widths set at 0.4 mm and 1.2 nm, respectively) as well as a Perkin-Elmer, model Lambda 9 spectrophotometer. The latter instrument was used to check for the presence of any low intensity bands, which could not be detected by the less sensitive instruments.

Synthesis of $[NiL^1H_{-1}]^+ClO_4^-$ crystals

0.10 g (0.37 mmol) of L^1 was dissolved initially in 5.0 cm^3 of 0.1 mol dm^{-3} HCl and 10.0 cm^3 of absolute methanol. To this ligand solution was added 18.3 cm^3 of 0.020 mol dm^{-3} $NiCl_2·6H_2O$ followed by 5.0 cm^3 of 0.1 mol dm^{-3} NaOH to adjust the pH to 7.15. The mixture was stirred at room temperature for 2 h after which a yellow mixture resulted. Addition of an excess of $NaClO_4$ solution to this yellow mixture resulted in the formation of a colloidal precipitate. After 5 days the desired orange–yellow complex crystallised out of solution. The crystals were filtered off, washed with small amounts of acetone and dried over anhydrous $CaCl_2$. Yield 0.08 g (51%).

CAUTION: Although no problems were encountered in the preparation of $[NiL^1H_{-1}]ClO_4$, perchlorate salts are potentially explosive and should be handled in small quantities with care.

Crystal-structure determination

An orange–yellow crystal (approximately 0.25 × 0.23 × 0.20 mm) of $[NiL^1H_{-1}]^+ClO_4^-$ was mounted on a Nonius Kappa CCD diffractometer equipped with a graphite-crystal monochromator. Unit cell determinations and data collections were performed with Mo-Kα radiation (λ = 0.71073 Å). A Lorentz-polarisation correction was applied to the data, as well as a semi-empirical absorption correction based on equivalent reflections (minimum and maximum absorption transmissions were 0.7445 and 0.7875, respectively). The structure was solved by direct methods (SHELXS-97, 1990[42]) and refined using full-matrix least-squares on F^2 (SHELXL-97, 1997[43]). Non-hydrogen atoms were treated anisotropically while hydrogen atoms were placed in geometrically calculated positions and linked to common thermal parameters.

Crystallographic data. $C_{13}H_{27}N_4O_2Ni·ClO_4$ (M_r 429.55): orthorhombic, space group *Pbca*, a = 13.396(1), b = 12.349(1), c = 21.933(1) Å, V = 3628.3(4) $Å^3$, Z = 8, μ = 1.254 mm^{-1},

D_c = 1.573 g cm^{-3}, T = 197 K. 18035 Reflections were collected of which 4146 were independent and 3439 were observed [$I > 2\sigma(I)$]. Refinement converged with $R1$ = 0.0294, wR = 0.0664 for observed data and $R1$ = 0.0417, wR = 0.0708 for all data.

CCDC reference number 211481.

See http://www.rsc.org/suppdata/dt/b4/b405756m/ for crystallographic data in CIF or other electronic format.

Model building and molecular dynamics (MD) simulations

Model building of the ligand and the corresponding starting complex was based on the crystal structure of [NiL^{1}H$_{-1}$]. This was accomplished by making use of fragments within the BUILDER module of the Biosym/MSI's II software package.[38] Structures were then optimised prior to dynamics runs to remove the strain using the SHAKE algorithm with the default ESFF force fields. The optimisation procedure in essence constrained all the bond lengths to their equilibrium value while a constant temperature algorithm was used to keep the temperature at 298 K. MD simulations of the complex species were performed by the DISCOVER_3 module (98 Version) which is run as an application in the INSIGHT II package.[38] The MM calculations and MD simulations were performed on a Silicon Graphics Indigo computer.

Acknowledgements

The authors are grateful to the National Research Foundation (NRF) and the Councils of the Universities of Transkei and Cape Town for financial support and a bursary to T. E. N.

References

1 R. Cammack and M. N. Hughes, in *Encyclopedia of Inorganic Chemistry*, ed.-in chief, R. B. King, John Wiley and Sons Ltd., Baffins Lane, Chichester, West Sussex, PO19 IUD, England, vol. 5, 1994, p. 2384; http://www.nutrition.org/nutinfo/content/nick.shtml; F. A. Cotton and G. Wilkinson, *Advanced Inorganic Chemistry (A Comprehensive Text)*, John Wiley and Sons Inc., NY, 4th edn., 1980, p. 1344.
2 G. E. Jackson and B. S. Nakani, *J. Chem. Soc., Dalton Trans.*, 1996, 1373.
3 T. E. Nomkoko, PhD Thesis, University of Cape Town, 2002.
4 E. T. Nomkoko, G. E. Jackson and B. S. Nakani, *Inorg. Chem. Commun.*, 2003, **6**, 335.
5 T. E. Nomkoko, G. E. Jackson, B. S. Nakani, W. K. A. Louw and J. R. Zeevaart, *Dalton Trans.*, 2004, 741.
6 T. E. Nomkoko, G. E. Jackson and B. S. Nakani, *Dalton Trans.*, 2004, 1432.
7 P. M. May, P. W. Linder and D. R. Williams, *J. Chem. Soc., Dalton Trans*, 1977, 588.
8 G. E. Jackson, P. M. May and D. R. Williams, *J. Inorg. Nucl. Chem*, 1978, **40**, 1227; G. Berthon, B. Hacht, M. Blais and P. M. May, *Inorg. Chim. Acta*, 1986, **125**, 219.
9 M. Micheloni, P. Paoletti and A. Sabatini, *J. Chem. Soc., Dalton Trans.*, 1983, 1189.
10 B. S. Nakani and R. D. Hancock, *S. Afr. J. Chem.*, 1983, **36**, 117.
11 P. M. May, K. Murray and D. R. Williams, *Talanta*, 1985, **35**, 825.
12 G. C. de Witt, P. M. May, J. Webb and G. Hefter, *Inorg. Chim. Acta.*, 1998, **275–276**, 37.
13 E. Bottari, A. Braibandi, L. Ciavatta, A. Corrie, P. Daniele, F. Dallavalle, M. Grimaldi, A. Mastroianni, G. Mori, G. Ostacoli, P. Paoletti, E. Rizzarelli, S. Sammartano, C. Severini, A. Vacca and D. Williams, *Ann. Chim. (Rome)*, 1978, **68**, 813.
14 K. Murray and P. M. May, *ESTA (Equilibrium Simulation for Titration Analysis) Manual*, University of Wales Institute of Science and Technology, Cardiff, 1984.
15 P. M. May, K. Murray and D. R. Williams, *Talanta*, 1988, **35**, 927.
16 R. K. Murmann, *J. Am. Chem. Soc.*, 1957, **79**, 521.
17 J. W. Fraser, G. R. Hedwig, H. K. J. Powell and W. T. Robinson, *Aust. J. Chem.*, 1972, **25**, 747.
18 C. Jubert, A. Mohamadou, C. Gerard, S. Brandes, A. Tabard and J.-P. Barbier, *J. Chem. Soc., Dalton Trans.*, 2002, 2660.
19 X. H. Bu, D. L. An, X. C. Cao, R. H. Zhang, T. Clifford and E. Kimura, *J. Chem. Soc., Dalton Trans.*, 1998, 2247.
20 C. F. Baes, Jr. and R. E. Mesmer, *The Hydrolysis of Cations*, Wiley-Interscience, New York, 1976, p. 241.
21 A. M. Duda, A. Karaczyn, H. Kozlowski, I. O. Fritsky, T. Glowiak, E. V. Prisyazhnaya, T. Yu. Sliva and J. Swiatek-Koslowska, *J. Chem. Soc., Dalton Trans.*, 1997, 3853.
22 V. Amendola, L. Fabbrizzi, C. Mangano, P. Pallavicini, A. Perotti and A. Taglietti, *J. Chem. Soc., Dalton Trans.*, 2000, 185.
23 A. E. Martell and R. D. Hancock, *Metal Complexes in Aqueous Solutions*, Plenum Press, New York, 1996, p. 1; R. D. Hancock and A. E. Martell, *Chem. Rev.*, 1989, **89**, 1875.
24 A. S. De Sousa, R. D. Hancock and J. H. Reibenspies, *J. Chem. Soc., Dalton Trans.*, 1997, 2831.
25 P. Comba, A. Fath, A. Kuhner and B. Nuber, *J. Chem. Soc., Dalton Trans.*, 1997, 1889.
26 R. D. Hancock, B. S. Nakani and F. Marsicano, *Inorg. Chem.*, 1983, **22**, 2531.
27 K. Kobiro, A. Nakayama, T. Hiro, M. Suwa and Y. Tobe, *Inorg. Chem.*, 1992, **31**, 676.
28 P. Planinic, D. M.-Calogovic and H. Meider, *J. Chem. Soc., Dalton Trans.*, 1997, 3445.
29 R. W. Hay and P. R. Norman, *Inorg. Chim. Acta.*, 1980, **45**, L139.
30 L. Hertli and T. A. Kaden, *Helv. Chim. Acta.*, 1981, **64**, 33.
31 J. R. Roper and H. Elias, *Inorg. Chem.*, 1992, **31**, 1202.
32 E. G. Vassian and R. K. Murmann, *Inorg. Chem.*, 1967, **6**, 2043.
33 A. B. P. Lever, *Studies in Physical and Theoretical Chemistry–Inorganic Electronic Spectroscopy*, Elsevier, Amsterdam, 2nd edn., 1984, p. 507.
34 E. A. Enyedy, H. Csoka, I. Lazar, G. Micera, E. Garriba and E. Farkas, *J. Chem. Soc., Dalton Trans.*, 2002, 2632.
35 M. J.-Bojczuk, W. Lesniak, W. Szczepanik, K. Gatner, A. Jezierski, M. Smoluch and W. Bal, *J. Inorg. Biochem.*, 2001, **84**, 189.
36 *Cambridge Structural Database Version 5.24 (November 2002)*, Cambridge Crystallographic Data Centre, University Chemical Laboratory, Cambridge, UK.
37 M. S. Hussain and E. O. Schlemper, *Inorg. Chem.*, 1979, **18**, 2275.
38 *Insight II User Guide*, October 1995, Biosym/MSI, San Diego.
39 A. I. Vogel, *Vogel's Textbook of Quantitative Inorganic Analysis*, Longman Group, London, 4th edn., 1978, p. 236 (revised by: J. Bassett, R. C. Denney, G. H. Jeffery and J. Mendham).
40 G. Gran, *Acta Chem. Scand.*, 1950, **4**, 559.
41 G. Gran, *Analyst.*, 1952, **77**, 661.
42 G. M. Sheldrick, *Acta Crystallogr., Sect. A*, 1990, **46**, 467.
43 G. M. Sheldrick, SHELXL 97, Suite of programs for crystal structure determinations, University of Göttingen, 1997.